arXiv:1404.5166v1 [cond-mat.mtrl-sci] 21 Apr 2014

Quasiparticle level alignment for photocatalytic interfaces

Annapaoala Migani,*,†,‡ Duncan J. Mowbray,*,‡ Jin Zhao,¶,§ Hrvoje Petek,‖ and Angel Rubio*,‡

†ICN2 - Institut Català de Nanociència i Nanotecnologia and CSIC - Consejo Superior de Investigaciones Cientificas, ICN2 Building, Campus UAB, E-08193 Bellaterra (Barcelona), Spain

‡Nano-Bio Spectroscopy Group and ETSF Scientific Development Center, Departamento de Física de Materiales, Centro de Física de Materiales CSIC-UPV/EHU-MPC and DIPC, Universidad del País Vasco UPV/EHU, E-20018 San Sebastián, Spain

¶Department of Physics and ICQD/HFNL, University of Science and Technology of China, Hefei, Anhui 230026, China

§Synergetic Innovation Center of Quantum Information & Quantum Physics, University of Science and Technology of China, Hefei, Anhui 230026, China

‖Department of Physics and Astronomy, University of Pittsburgh, Pittsburgh, Pennsylvania 15260, USA

ABSTRACT: Electronic level alignment at the interface between an adsorbed molecular layer and a semiconducting substrate determines the activity and efficiency of many photocatalytic materials. Standard density functional theory (DFT) based methods have proven unable to provide a quantitative description of this level alignment. This requires a proper treatment of the anisotropic screening, necessitating the use of quasiparticle (QP) techniques. However, the computational complexity of QP algorithms has meant a quantitative description of interfacial levels has remained elusive. We provide a systematic study of a prototypical interface, bare and methanol covered rutile TiO_2(110) surfaces, to determine the type of many-body theory required to obtain an accurate description of the level alignment. This is accomplished via a direct comparison with metastable impact electron spectroscopy (MIES), ultraviolet photoelectron spectroscopy (UPS) and two-photon photoemission (2PP) spectra. We consider GGA DFT, hybrid DFT and G_0W_0, scQP$GW1$, scQPGW_0, and scQPGW QP calculations. Our results demonstrate that G_0W_0, or our recently introduced scQP$GW1$ approach, are required to obtain the correct alignment of both highest occupied and lowest unoccupied interfacial molecular levels (HOMO/LUMO). These calculations set a new standard in the interpretation of electronic structure probe experiments of complex organic molecule–semiconductor interfaces.

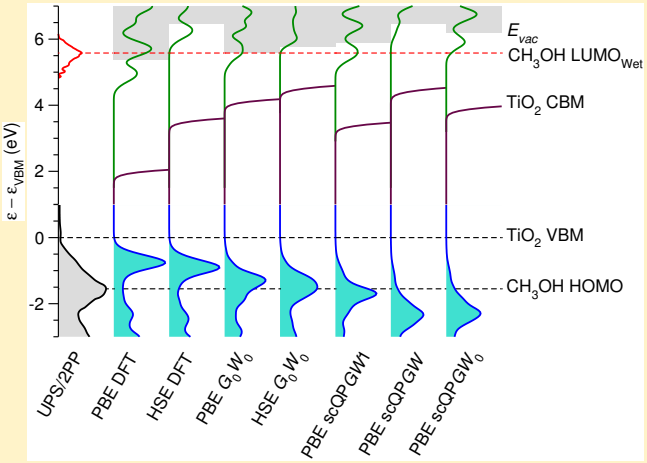

INTRODUCTION

Describing the level alignment in photocatalytic materials is a fundamental first step in their development into technology. This requires a quantitative description of the levels associated with the interface between a solid semiconductor and an adsorbed organic molecule. The alignment of the frontier highest occupied and lowest unoccupied molecular orbitals (HOMO/LUMO) with the valence band maximum (VBM) and conduction band minimum (CBM) of the semiconducting substrate controls the interfacial electron transfer.[1,2] Such electron transfer is necessary for a system to be photocatalytically active.

For a theoretical technique to be robust for describing the interface, ideally, it would reproduce the electronic and optical band gaps, along with the optical spectra of the bulk material. Further, the alignment of the VBM and CBM of the bare surface would be reproduced. These requirements could then be used to justify the use of a theoretical technique for an interfacial system. Only by reproducing the measured level alignment may we provide a robust theoretical interpretation.

The accurate description of level alignment requires techniques which incorporate the spatial dependence of the electron-electron correlation. This is especially important for the interface, as it includes both the vacuum and the bulk substrate. For unoccupied levels located in the vacuum above the surface there is little to no electronic screening. This is already described by the bare Hartree term within standard density functional theory (DFT). For unoccupied levels located within a semiconducting substrate, electronic screening can be quite significant. This can be described by a constant screening of the Hartree-Fock exact-exchange term, as done via the fraction of exact-exchange included within hybrid DFT exchange and correlation (xc)-functionals.[3] However, for unoccupied interfacial levels, with weight in both the vacuum and substrate, the screening is intermediate and spatially heterogeneous. This anisotropy of the electron-electron correlation can be described using many-body quasiparticle (QP) techniques.[4–6] This anisotropic screening is even more important for the levels of a molecular monolayer (ML) on a semiconducting substrate, e.g. image states[7] or wet electron levels.[8]

Despite its importance, computations of interfacial levels employing QP techniques are scarce.[8–13] This is mainly due to the difficulty in carrying out QP calculations on atomistic models with hundreds of atoms, as they are computationally prohibitive. Here, we apply QP techniques to the accurate computation of the inter-

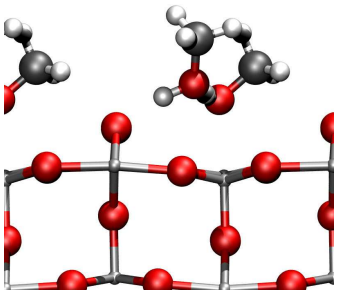

Figure 1. Schematic of the most stable geometry for a CH_3OH ML on a TiO_2(110) surface from ref. 29. H, C, O, and Ti atoms are represented by white, grey, red, and silver balls, respectively. Adapted with permission from ref. 8. Copyright 2013 American Chemical Society.

face between rutile TiO_2(110) and methanol. Methanol is chosen for its important applications in photocatalysis (direct photocatalytic dissociation,[14,15] hydrogen formation,[16] photo-oxidation to formaldehyde[17] or methyl formate[18,19]) and photoelectrocatalysis (as a sacrificial agent[20] in oxidative dehydrogenation of water[21,22]). Viewed from a theoretical perspective, methanol on TiO_2(110) represents one of the "simplest" and computationally feasible systems for applying QP *GW* calculations to an entire interface.[8,9]

Many studies have probed the electronic structure and photocatalytic activity of methanol on the single crystal rutile TiO_2(110) surface under ultra-high vacuum (UHV) conditions. Experimentalists have employed a full arsenal of techniques, such as ultraviolet, X-ray, and two photon photoemission spectroscopy (UPS, XPS, and 2PP),[14,19,23–25] scanning tunnelling microscopy[14,26,27] (STM), and mass spectrometric analysis of reaction products.[17,18,28] A proper interpretation of these results requires a similar arsenal of robust theoretical techniques for their explanation.

In this article we apply many-body QP techniques (G_0W_0,[30] scQP*GW*1,[8] scQP*GW*,[31–33] or scQPGW_0[34]) to bulk (rutile TiO_2), surface (TiO_2(110)), and interfacial (CH_3OH ML on TiO_2(110) shown in Figure 1) systems. These are based on DFT calculations using either a local density approximation (LDA),[35] generalized gradient approximation (PBE)[36] or hybrid (HSE)[37] xc-functional. For the interface, the HSE G_0W_0 results of the present study are compared with those we reported previously in refs. 8 and 38. Through this detailed comparison, our aim is to demonstrate not only which techniques provide the best description of the level alignment, but also why. To accomplish this, we directly compare with: (1) the dielectric function probed by optical reflectivity[39] and ellipsometry[40] experiments for the bulk; (2) the work function probed by metastable impact electron spectroscopy (MIES)[41] for the surface; and (3) the occupied molecular levels probed by UPS[23] experiments and the unoccupied molecular levels probed by 2PP[14,24,42,43] experiments for the interface.

It is the alignment of these molecular levels with the VBM and CBM which controls the photocatalytic activity of the interface. However, for titania it is rather difficult for a single technique to describe the electronic and optical band gaps, optical spectra, and surface work function (i.e. VBM and CBM relative to the vacuum level) simultaneously. We will show that a mixture of several techniques is necessary to obtain a complete description of the level alignment of titania bulk, surface, and interfacial systems.

METHODOLOGY

We begin by providing a brief description of the various QP techniques in Section 2.1. The specific computational parameters employed for bulk, surface, and interface systems are then listed in Section 2.2. Finally, in Section 2.3 we describe how energy references are obtained from the experimental data.

2.1. Theoretical Methods. The QP G_0W_0 approach involves the single-shot correction of the DFT eigenvalues by the self energy $\Sigma = iGW$, where G is the Green's function and W is the screening.[4] W is obtained from the dielectric function, based on the Kohn-Sham wavefunctions.[5] This is calculated using linear response time-dependent DFT within the random phase approximation (RPA), including local field effects.[30] Although one obtains a first-order approximation to the QP eigenvalues within G_0W_0, this technique provides no information on how screening affects the energy of the vacuum level, E_{vac}, and the spatial distribution of the wavefunctions, i.e. the QP wavefunctions. For image potential levels and wet electron levels the QP wavefunctions are qualitatively different from their Kohn-Sham counterparts,[7] motivating the use of self-consistent *GW* techniques.

In the self-consistent procedure we use,[31–33] the QP wavefunctions at each iteration are obtained by diagonalizing the Hermitian part of the Hamiltonian and overlap matrices in the basis of the previous step's wavefunctions. Here, we denote this methodology by "scQP*GW*" as opposed to "sc*GW*". This is to provide a clear distinction from self-consistent *GW* calculations where the full Hamiltonian is diagonalized.[44]

At the scQP*GW* level, self-consistent *GW* calculations are performed until full self consistency is obtained for the QP eigenvalues.[33,34] This method has been found to significantly overestimate band gaps for most materials.[33]

The scQPGW_0 technique has been proposed to partly remedy scQP*GW*'s tendency to overestimate band gaps.[33,34] In scQPGW_0 the screening W is fixed to that obtained within RPA based on the Kohn-Sham wavefunctions, i.e. W_0. This is justified by the fact that DFT typically yields reliable dielectric constants.[34]

In fact, the overestimation of band gaps by self-consistent *GW* calculations has recently been attributed to the neglect of the lattice polarization contribution to the screening of the electron-electron interaction.[45] This effect has been shown to always reduce the band gap, and is particularly significant for polar materials such as TiO_2. Overall, the good performance of G_0W_0 is attributable to "a partial cancellation of errors: the underestimation of the band gap opening is compensated by the neglect of the band gap shrinkage due to the lattice polarization", as stated in ref. 45.

For this reason, we have recently introduced the scQP*GW*1 approach.[8] The self energy corrections must be applied in small fractions to obtain a smooth convergence of the QP wavefunctions during the self-consistent cycle. At each step, the eigenvalues and wavefunctions are computed and updated for the subsequent step. This means one may choose to stop the self-consistent procedure once a full portion of QP self energy has been introduced. At this point the xc-potential has been completely replaced by self energy. In this way one obtains QP eigenvalues comparable to those from G_0W_0, along with the QP wavefunctions and vacuum level. If instead the full self energy correction is applied in one step, entirely replacing the xc-potential, one would obtain the same QP eigenvalues as from G_0W_0. Here the vacuum level is obtained from the Hartree and ionic electrostatic contributions to the effective potential far from the surface. In general, scQP*GW*1 is expected to provide an accurate description of all materials for which G_0W_0 calculations have proven successful.

It has previously been shown[38,46–48] that the experimental op-

tical spectra for bulk rutile TiO_2 may be obtained via the Bethe-Salpeter equation (BSE)[49] based on G_0W_0 eigenvalues. The electrostatic electron-hole interaction is included using an effective nonlocal frequency independent exchange correlation $f_{xc}(\mathbf{r},\mathbf{r}',\omega = 0)$ kernel suggested in ref. 50.

Similarly, the test charge/test charge scQP*GW* scheme, scQPGW^{TCTC}, includes electrostatic electron-hole interactions, i.e. vertex corrections, within the computation of the screening W.[33] This is again accomplished by including $f_{xc}(\mathbf{r},\mathbf{r}',\omega = 0)$ within the dielectric function, as described in ref. 50. In this work we have applied the scQPGW^{TCTC} scheme starting from the converged scQP*GW* results.

2.2. Computational Details. All calculations have been performed using the DFT code VASP within the projector augmented wave (PAW) scheme.[51] We used either a localized density approximation (LDA)[35] (bulk), generalized gradient approximation (PBE)[36] (surface/interface) or a range separated hybrid functional (HSE)[37] (surface/interface) for the xc-functional.[52] In particular, we use the HSE06 variant, with a screening parameter of $\mu = 0.2$ Å^{-1}, of the HSE hybrid xc-functional, which includes 25% exact-exchange.[37] The geometries have been fully relaxed, with all forces $\lesssim 0.02$ eV/Å, a plane-wave energy cutoff of 445 eV, an electronic temperature $k_BT \approx 0.2$ eV with all energies extrapolated to $T \to 0$ K, and a PAW pseudopotential for Ti which includes the $3s^2$ and $3p^6$ semi-core levels.[47]

Bulk. The G_0W_0 calculations for bulk rutile TiO_2 are based on DFT calculations performed using the LDA[35] xc-functional. A $4.5941 \times 4.5941 \times 2.958$ Å^3 unit cell with D_{2h} symmetry, corresponding to the experimental lattice parameters for bulk rutile TiO_2, was employed. A Γ centered **k**-point mesh of $6 \times 6 \times 10$ was used, yielding a sampling of 0.228 Å^{-1} in the (100)/(010) directions and 0.212 Å^{-1} in the (001) direction of the Brillouin zone. The electronic density and wave functions were calculated with an increasing number of unoccupied bands per atom, $n_{\mathrm{unocc}} = 12$, 22 2/3, 38 2/3, 49 1/3, 65 1/3, 76, 102 2/3, 129 1/3, and 150 2/3, i.e. including all levels up to 52, 85, 127, 151, 184, 204, 357, 392, and 428 eV above the VBM, respectively, to converge the calculation at the G_0W_0 level. We used an energy cutoff for the number of **G**-vectors for representing the response function of 297 eV, and 192 sampling points for the RPA dielectric function.

As a further comparison, we have performed similar G_0W_0 calculations for bulk rutile TiO_2 using the Grid-based PAW code GPAW.[53,54] Here we used a $7 \times 7 \times 11$ **k**-point mesh, a $h \approx 0.2$ Å grid spacing, an energy cutoff for the number of **G**-vectors for representing the response function of 100 eV, and 73 sampling points for the RPA dielectric function.

The scQP*GW*1 calculations for bulk rutile TiO_2 are based on DFT calculations performed using the LDA[35] and HSE[37] xc-functionals including $n_{\mathrm{unocc}} = 12$ unoccupied bands per atom.

For the BSE calculations we used a denser Γ-centered $8 \times 8 \times 12$ **k**-point mesh and 480 sampling points for the RPA dielectric function. We included $n_{\mathrm{unocc}} = 12$ unoccupied bands per atom for the G_0W_0 calculation, and included transitions between 12 occupied and 16 unoccupied bands in the BSE calculation.[49]

Surface. The G_0W_0, scQP*GW*1, scQP*GW*, and scQPGW^{TCTC} calculations for rutile TiO_2(110) are based on DFT calculations performed using the PBE[36] and HSE[37] xc-functionals, with scQPGW_0 based on PBE. We used a four layer pristine TiO_2(110) 1×1 unit cell of $6.497 \times 2.958 \times 40$ Å^3 with a vacuum separation of 27 Å. We employed a Γ-centered $4 \times 8 \times 1$ **k**-point mesh, 320 bands = 91/3 unoccupied bands per atom, i.e. including all levels up to 26 eV above the VBM, an energy cutoff of 80 eV for the number of **G**-vectors, and a sampling of 80 frequency points for the dielectric function.

The electronic density and wave functions were also calculated with an increasing number of unoccupied bands per atom, $n_{\mathrm{unocc}} = 22\,2/3$, $38\,2/3$, $49\,1/3$, $65\,1/3$, and 76, i.e. including all levels up to 46, 66, 77, 93, and 103 eV above the VBM, respectively, to converge the calculation at the G_0W_0 level.

As a further check, we performed PBE G_0W_0 calculations for an eight layer pristine TiO_2(110) 1×1 unit cell of $6.497 \times 2.968 \times 53$ Å^3 with a vacuum separation of 27 Å. We used either $9\,1/3$ or 76 unoccupied bands per atom, i.e. including all levels up to 32 or 134 eV above the VBM.

Interface. The G_0W_0 calculations for CH_3OH on TiO_2(110) are based on DFT calculations performed using the PBE[36] and HSE[37] xc-functionals, with scQP*GW*1, scQP*GW*, scQPGW_0 based on PBE. We modelled the most stable monolayer structure of CH_3OH on TiO_2(110)[29] with adsorbates on both sides of a four layer slab, with C_2 symmetry. We used a 1×2 unit cell of $6.497 \times 5.916 \times 47.0$ Å^3, corresponding to the experimental lattice parameters for bulk rutile TiO_2[55] in the surface plane. This provides $\gtrsim 27$ Å of vacuum between repeated images. We employed a Γ centered $4 \times 4 \times 1$ **k**-point mesh, with 880 bands = $9\,1/6$ unoccupied bands per atom, i.e. including all levels up to 30 eV above the VBM, an energy cutoff of 80 eV for the number of **G**-vectors, and a sampling of 80 frequency points for the dielectric function.

2.3. Experimental Energy References. Experimental spectra are typically referred to the Fermi level, ε_F, which is pinned about 0.1 eV below the CBM for mildly reduced TiO_2.[56–58] Using the experimental work function $\phi \approx 5.3 - 5.5$ eV,[23,41,59,60] one may obtain the CBM energy relative to the vacuum level of $\varepsilon_{\mathrm{CBM}} \approx -\phi + 0.1 \approx -5.2$ or -5.4 eV. Similarly, using the electronic band gap for rutile TiO_2 of 3.3 ± 0.5 eV obtained from electron spectroscopy measurements,[61] one may estimate the VBM energy relative to the vacuum level at $\varepsilon_{\mathrm{VBM}} \approx -\phi + 0.1 - 3.3 \approx -8.5$ or -8.7 eV. For bare TiO_2(110) we have used these references to compare with the computed VBM and CBM energies relative to the vacuum level.

For the interface, the workfunction is strongly dependent on the structure of the adsorbing CH_3OH ML, i.e. $\Delta\phi \sim 0.9$ eV.[29] Moreover, the VBM is the most reliable theoretical reference. For these reasons, we have aligned the experimental UPS and 2PP spectra for the interface to the VBM. This is done by adding the value for the Fermi level relative to the VBM, i.e., $\varepsilon_F \approx -0.1 + 3.3 = 3.2$ eV. In this way we are able to directly compare the methanol occupied and unoccupied densities of states we calculate with the UPS and 2PP spectra.

RESULTS AND DISCUSSION

For a theoretical technique to be robust for describing interfacial level alignment, it would ideally reproduce the electronic properties of the bulk material and bare surface. With these ideas in mind, we discuss in Section 3.1 the convergence of the electronic and optical band gap, along with the optical spectra, for bulk rutile TiO_2. Based on these results, we compare the performance of various QP techniques for describing the VBM and CBM level alignment for the bare TiO_2(110) surface in Section 3.2. We then show in Section 3.3 which of these techniques provide the best agreement with the UPS and 2PP spectra for a CH_3OH ML on TiO_2(110). Finally, in Section 3.4 we show how the QPG_0W_0 energy corrections are correlated with the spatial distribution of the wave functions.

3.1. Electronic and Optical Band Gap of Bulk Rutile TiO_2. The first robustness criteria we shall consider is the electronic and optical band gap description for bulk rutile TiO_2. This also includes a comparison between the calculated and measured optical spectra.

As shown in Figure 2, to obtain a reasonable convergence of the direct and indirect band gaps for bulk TiO_2 requires about $n_{\mathrm{unocc}} \approx 76$ unoccupied bands per atom. The convergence with the

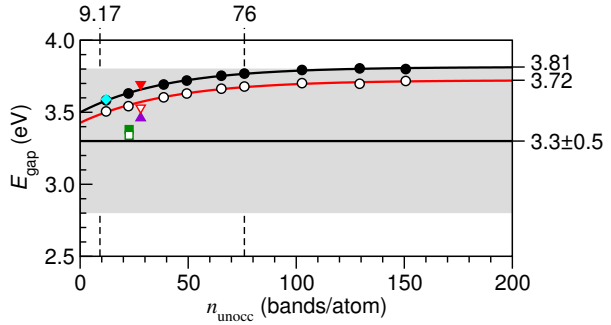

Figure 2. Convergence of the TiO_2 bulk rutile G_0W_0 direct (filled symbols) and indirect (open symbols) band gaps, E_{gap}, with the number of unoccupied bands per atom, n_{unocc}. Exponential fits (solid lines) yield asymptotic limits of 3.81 and 3.72 eV for the direct and indirect band gaps, respectively. Results are from this work with VASP (black circles), GPAW (red triangle down), ref. 46 (cyan diamond), ref. 47 (green squares), and ref. 48 (violet triangle up). The experimental electronic band gap of 3.3 ± 0.5 eV from ref. 61 is provided for comparison.

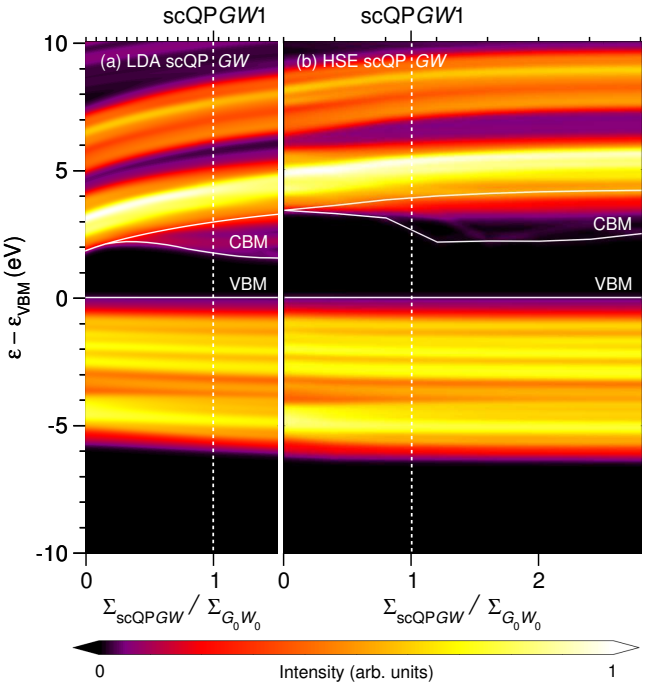

Figure 3. Convergence of the DOS for bulk rutile TiO_2 with respect to the cumulative sum of portions of self energy introduced self-consistently, $\Sigma_{scQPGW}/\Sigma_{G_0W_0}$, from (a) LDA scQP$GW$ and (b) HSE scQPGW. Energies ε in eV are taken relative to the VBM ε_{VBM}. White solid lines indicate the VBM and CBM positions for the direct and indirect gaps. White dashed lines indicate the DOS corresponding to scQPGW1 results. Upper ticks indicate the steps of the scQPGW calculations.

number of unoccupied bands is quite well described by a simple exponential fit, i.e. $E_\infty + \alpha \exp(-n_{unocc}/\beta)$. From this we obtain the asymptotic limits of 3.72 eV and 3.81 eV for the direct and indirect gap, respectively.

Figure 3 shows the convergence of the total density of states (DOS) with respect to the cumulative sum of portions of self energy introduced self-consistently with the QP LDA and HSE scQPGW calculations. The upper ticks in Figure 3 denote the steps at which the eigenvalues and QP wavefunctions are calculated. The intermediate DOS are obtained by linearly interpolating betweeen the calculated eigenvalues at each step. At Γ the LDA DOS at $\Sigma_{scQPGW}/\Sigma_{G_0W_0} = 1.5$ approaches the HSE DFT DOS. The direct band gap at $\Sigma_{scQPGW}/\Sigma_{G_0W_0} = 2.8$ for HSE scQPGW

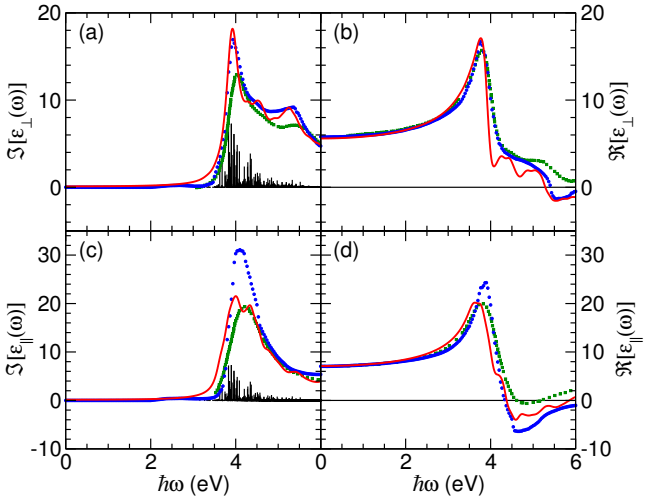

Figure 4. Calculated imaginary (a,c) and real (b,d) parts of the dielectric function of bulk rutile TiO_2 for polarization perpendicular (a,b) and parallel (c,d) to the TiO_2 tetragonal c-axis, $\Im[\varepsilon_\perp(\omega)]$,[38] $\Re[\varepsilon_\perp(\omega)]$, $\Im[\varepsilon_\parallel(\omega)]$, and $\Re[\varepsilon_\parallel(\omega)]$, versus energy, $\hbar\omega$, in eV. The BSE spectra (red solid line) are based on G_0W_0 eigenvalues. The experimental spectra are obtained from the measured refractive index and absorption index from ref. 39 (blue circles) and ellipsometry measurements of the dielectric function from ref. 40 (green squares) at room temperature.

is $E_{gap} \approx 4.18$ eV, in agreement with the LDA scQPGW results of ref. 32. This is related to the starting-point independence of the scQPGW procedure.

The indirect band gap is significantly underestimated for both LDA and HSE bulk scQPGW calculations. We attribute this to the lack of hermiticity of the Hamiltonian for these **k**-points. This problem is more significant for LDA than HSE scQPGW calculations. We suggest this is because HSE DFT is closer to converged scQPGW than LDA DFT. Since the CBM levels which make up the indirect band gap are not present in a four layer slab model, these difficulties for the scQPGW method are not observed for the bare and CH_3OH covered TiO_2(110) surfaces.

G_0W_0 with a converged number of bands significantly overestimates the experimental band gap of 3.3 ± 0.5 eV,[61] although it is still within the upper limit of the experimental error. We attribute this overestimation of the electronic band gap to the neglect of lattice polarization contributions within the screening. This is expected to be quite important for polar materials such as titania.

The success of G_0W_0 for describing the electronic band gaps of polar materials is partly due to a cancellation of errors.[3] Performing GW self-consistently *increases* the G_0W_0 electronic gap, while including lattice polarization within the screening significantly *decreases* the electronic gap back to the G_0W_0 value. However, for titania the contribution of lattice polarization within the dielectric function is so significant that the electronic gap is already overestimated at the G_0W_0 level.

Including lattice polarization contributions within the screening requires a self-consistent GW calculation, and is not currently available. Instead, we have employed a semi-empirical approach.

As shown in Figure 2, the number of bands employed in previous calculations[46–48] is significantly smaller than that required to fully converge a G_0W_0 calculation. Taking the number of bands to be a "tuning" parameter, we have used a reduced number of unoccupied bands within the BSE calculation shown in Figure 4.

We find 12 unoccupied levels per atom yields a QP energy gap of 3.32 eV, in quantitative agreement with the experimental band gap of 3.3 ± 0.5 eV.[61] These G_0W_0 results have been used in the BSE

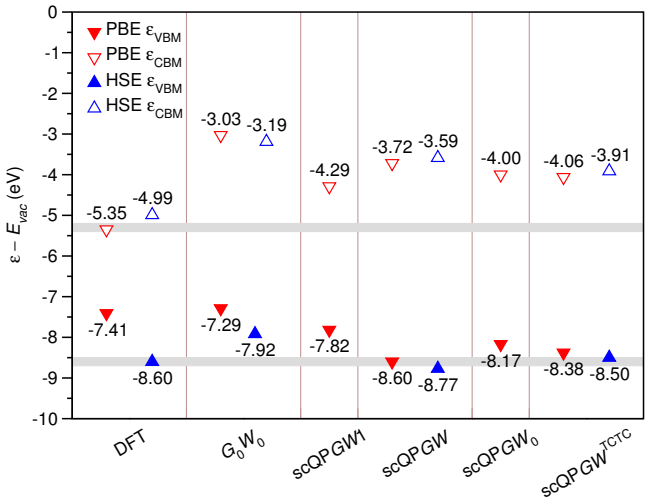

Figure 5. VBM and CBM energies, ε_{VBM} and ε_{CBM}, in eV for a bare TiO_2(110) surface relative to the vacuum level E_{vac} from DFT, G_0W_0, scQPGW1, scQPGW, scQPGW_0, and scQPGW^{TCTC} using PBE and HSE xc-functionals. Gray regions denote VBM and CBM energies derived from the experimental results as discussed in Section 2.3.

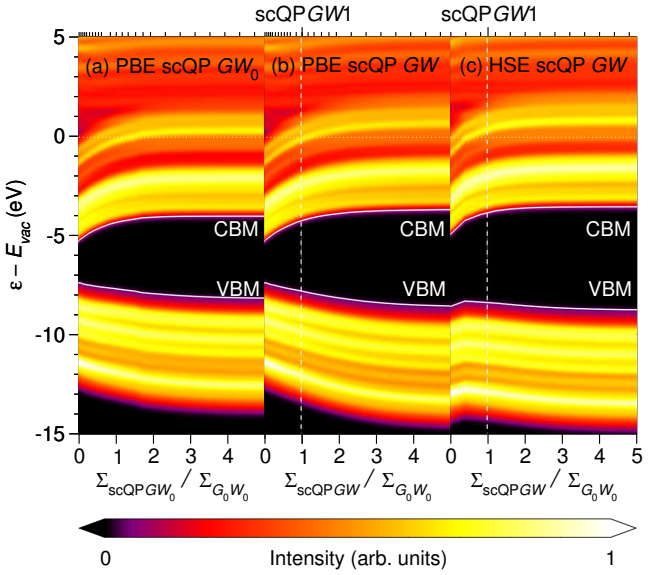

Figure 6. Convergence of the DOS for bare TiO_2(110) with respect to the cumulative sum of portions of self energy introduced self-consistently, $\Sigma_{scQPGW}/\Sigma_{G_0W_0}$, from (a) PBE scQP$GW_0$, (b) PBE scQP$GW$, and (c) HSE scQP$GW$. Energies ε in eV are taken relative to the vacuum level E_{vac} (white dotted line). White solid lines indicate the VBM and CBM positions. White dashed lines indicate the DOS corresponding to scQPGW1 results. Upper ticks indicate the steps of the (a) scQPGW_0 and (b,c) scQPGW calculations.

to calculate the optical absorption spectrum.

Figure 4 shows the imaginary and real parts of the dielectric function of bulk rutile TiO_2 for polarization perpendicular and parallel to the tetragonal axis c. This is calculated from the BSE while the experimental results are obtained from optical reflectivity[39] and ellipsometry[40] measurements at room temperature. The BSE results are in excellent agreement with experiment in both directions: the onsets, the intensities, the main peaks around 4 eV, the line shapes, the macroscopic dielectric function $\Re[\varepsilon(\omega = 0)]$, and the plasmon frequencies ω_p (i.e. where $\Re[\varepsilon(\omega_p)] = 0$) are all well reproduced. Further, our G_0W_0 and BSE calculations for bulk rutile TiO_2 agree with those reported previously.[46–48]

Overall, the success of this semi-empirical approach for the bulk is demonstrated by reproducing the electronic and optical band gaps along with the optical spectrum. Given the success of this strategy for the bulk, we apply a similarly reduced number of unoccupied bands per atom for our calculations of the surface and interface. Specifically, we perform QP calculations with $n_{unocc} = 9^1/_3$ and $9^1/_6$ per atom for the bare and CH_3OH covered TiO_2(110) surfaces, respectively. In this way, we expect to obtain an improved description of the titania level alignment at a significantly reduced computational cost.

3.2. Level Alignment for Bare Rutile TiO_2(110). The second robustness criteria we shall consider is the alignment of the VBM and CBM for the bare TiO_2(110) surface. The VBM and CBM alignment from DFT, G_0W_0, scQPGW1, scQPGW, scQPGW_0, and scQPGW^{TCTC} calculations using PBE and HSE xc-functionals is shown in Figure 5. These results are compared with the experimental references for the VBM and CBM discussed in Section 2.3.

As shown in Figure 5, the computed electronic band gap for bulk rutile TiO_2 is significantly smaller than that obtained from a TiO_2(110) four layer slab model. Overall, we find all self-consistent QP techniques describe the VBM level alignment consistently with experiment. This agrees with the improved description of molecular vertical ionization potentials obtained with self-consistent GW.[44] The band gap overestimation by self-consistent QP techniques is mostly reflected in an overestimation of the CBM energy. For G_0W_0 calculations the vacuum level is not accessible, so the alignment is relative to the DFT vacuum level. This lack of a well defined vacuum level negatively impacts the absolute energy alignment for G_0W_0. Calculating directly the QP vacuum level is a distinct advantage of self-consistent QP techniques.

DFT based on the HSE xc-functional (HSE DFT) reproduces the VBM and CBM to within 0.2 eV. The VBM of TiO_2(110) is composed of interior O 2p levels, while the CBM is composed of interior Ti 3d levels. As both the VBM and CBM are located within the bulk, a correct energy alignment of these levels requires an accurate description of electron-electron correlation within the bulk. HSE correlation is basically a constant screening, i.e. an optical dielectric constant of $\varepsilon_\infty \sim 4$, of the Hartree-Fock exact-exchange term.[3] This provides an improved description for bulk rutile TiO_2, for which the measured optical dielectric constants are $\varepsilon_{\infty,a} = 6.84$ and $\varepsilon_{\infty,c} = 8.43$ along the a-axis and c-axis, respectively.[62] For this reason, HSE works well for the VBM and CBM energy alignment. Note the RPA optical dielectric constants ($\varepsilon_{\infty,a} \approx 7.83$ and $\varepsilon_{\infty,c} \approx 9.38$)[63] provide a better description than HSE of the anisotropic screening in bulk rutile TiO_2. Since these anisotropies in the screening are still rather small for the bulk, HSE works reasonably well for the bare TiO_2(110) surface. However, for the interfacial levels of a CH_3OH ML on TiO_2(110), the anisotropies in the screening are quite important, as we will discuss in Section 3.3.

Figure 6 shows the convergence of the DOS with respect to the cumulative sum of portions of self energy introduced self-consistently with the QP PBE scQPGW_0, PBE scQPGW, and HSE scQPGW calculations. From the DFT results, shown to the left of each panel, as the DFT xc-potential is replaced by the self energy Σ, the gap between occupied and unoccupied levels is increased monotonically. Most of the correction to the electronic band gap is already introduced at the scQPGW1 level, i.e. when a total of one full "portion" of self energy has been included within the self-consistent cycles. Note that the oscillations observed for HSE scQPGW are related to the use of a larger step size when introducing the portions of self energy.

The QP energy corrections for the occupied levels mimic those of

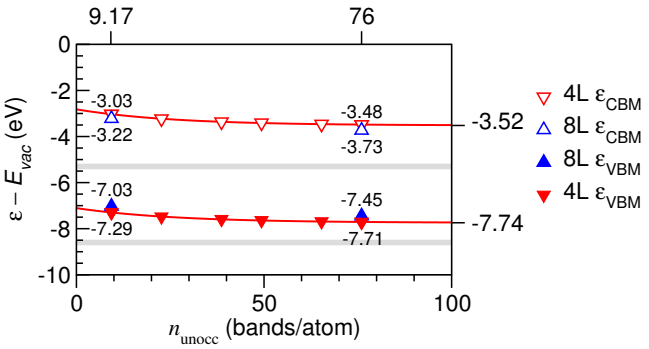

Figure 7. Convergence of the VBM and CBM energies, ε_{VBM} and ε_{CBM}, in eV for a bare four layer (4L) and eight layer (8L) TiO_2(110) surface relative to the vacuum level E_{vac} from G_0W_0, with the number of unoccupied bands per atom, n_{unocc}. Exponential fits (solid lines) yield asymptotic limits of −7.74 and −3.52 eV for the VBM and CBM, respectively. Gray regions denote VBM and CBM energies derived from the experimental results as discussed in Section 2.3.

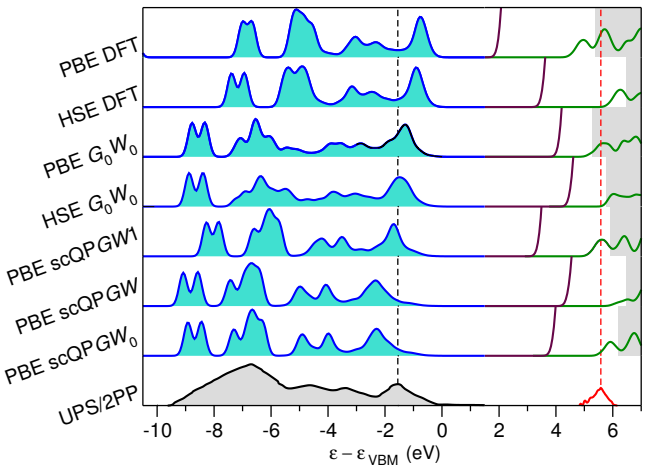

Figure 8. Total unoccupied (maroon), CH_3OH projected (blue), and Wet (green) DOS computed with PBE DFT,[38] HSE DFT,[38] PBE G_0W_0,[8] HSE G_0W_0, PBE scQPGW1,[8] PBE scQPGW,[38] PBE scQPGW_0[8] for an intact methanol monolayer on TiO_2(110) and the experimental UPS[23] (black) and 2PP spectra[42] (red). Filling denotes occupied levels. Energies are relative to the VBM, ε_{VBM}. Gray shaded regions denote levels above the vacuum level E_{vac}. Black/red dashed vertical lines denote the UPS/2PP highest and lowest energy peaks, respectively.

the VBM. Similarly the corrections for the unoccupied levels with weight in the bulk mimic those of the CBM. Altogether, this suggests that in the absence of defects, the screening of bulk levels is rather homogeneous for the bare surface. This means a constant dielectric screening of the Hartree-Fock exact-exchange term may be sufficient to describe the electron-electron correlation for the surface. This is exactly what is accomplished by hybrid xc-functionals such as HSE. This explains the near quantitative agreement for the level alignment with HSE DFT, shown in Figure 5.

However, unoccupied levels with a significant weight in the vacuum, i.e. vacuum levels, undergo quite small QP energy corrections. This is clearly seen from the flat profiles at $\varepsilon \gtrsim 1$ eV above E_{vac}. This is because there is no electronic screening for vacuum levels, so that the bare Hartree term of standard DFT already describes the electron-electron correlation quite well.

Comparing the PBE scQPGW_0 and scQPGW results of Figure 6 (a) and (b), we see that by fixing the screening to that obtained from DFT, we reach self-consistency earlier, and the opening of the band gap is significantly reduced. Moreover, Figure 6 (b) and (c) clearly show the fully converged scQPGW DOS is independent of the xc-functional (PBE or HSE) used at the DFT level. Using HSE at the DFT level one reaches self-consistency much earlier, and using larger steps than with PBE. Altogether, HSE and HSE G_0W_0 are closer to scQPGW than PBE and PBE G_0W_0.

As a further check, we show in Figure 7 the convergence with number of unoccupied bands of the PBE G_0W_0 VBM and CBM energies relative to the DFT vacuum level. We find the ionization potentials and electron affinities for the bare TiO_2(110) surface increase (~ 0.4 eV) with the number of unoccupied bands included in the G_0W_0 calculation. However, the calculated band gap for the four and eight layer surfaces are already converged for $n_{unocc} = 9^1/_3$. For four layers with $n_{unocc} = 9^1/_3$, $E_{gap} \approx 4.26$ eV compared to 4.22 eV in the asymptotic limit. When the number of layers is increased from four to eight, we obtain the bulk band gap for $n_{unocc} = 76$ of 3.72 eV. Although the eight layer slab model provides an improved description of the bulk TiO_2 band gap, a four layer model should be sufficient to describe the interfacial level alignment. This is because the interfacial levels are located primarily within the first few layers of the surface.[8,9,38]

The number of bands required to converge the band gap for the bare TiO_2(110) surface is much smaller than that needed for bulk rutile TiO_2. This may be due to the different nature of the unoccupied levels being added in G_0W_0 calculations for the bulk (e.g. Rydberg levels) and the bare surface (e.g. vacuum levels).

Overall, we find that the VBM of the bare TiO_2(110) surface is described in a consistent manner with experiment by most of the QP techniques considered herein. This is important because the workfunction for methanol covered surfaces is strongly dependent on the structure of the interface. Moreover, the VBM is the most reliable reference from a theoretical perspective. For these reasons, in Section 3.3 we carry out the level alignment relative to the VBM. Furthermore, this has the advantage of obtaining convergence of the electronic structure with as few as nine unoccupied bands per atom.

3.3. Level Alignment for a CH_3OH ML on TiO_2(110). In Sections 3.1 and 3.2 we discussed the performance of the various QP techniques for describing level alignment with homogeneous screening, i.e., pristine bulk rutile TiO_2 and the bare TiO_2(110) surface. We now consider the performance of the same QP techniques for the alignment of interfacial levels undergoing anisotropic screening, i.e., the CH_3OH ML on TiO_2(110) interface shown in Figure 1. Specifically, in Figure 8, we compare the CH_3OH PDOS and Wet DOS computed with PBE DFT, HSE DFT, PBE G_0W_0, HSE G_0W_0, PBE scQPGW1, PBE scQPGW, and PBE scQPGW_0, with UPS and 2PP spectra for a CH_3OH ML on TiO_2(110).

UPS experiments[23] have probed the occupied molecular levels for the CH_3OH ML on TiO_2(110) interface. As shown in ref. 8 and depicted in Figure 9, the higher energy occupied molecular levels (HOMOs) are composed of non-bonding O 2p orbitals of the CH_3OH molecules, with some C–H σ and Ti 3d character. We have previously shown[8] that the highest energy peak in the UPS, at $\varepsilon^{UPS}_{peak} \approx -1.55$ eV relative to the VBM, is due to these HOMO levels.

Likewise 2PP experiments[14,24,25] have probed the unoccupied molecular levels for the CH_3OH ML on TiO_2(110) interface. As shown in ref. 8 and depicted in Figure 9, these unoccupied molecular levels have a primarily two dimensional (2D) σ^* character associated with the methanol C–H bond, with weight above the H atoms outside the molecular layer (brown regions).[24] We have previously shown[8] that it is these "Wet electron" levels[25] of intact (i.e., undissociated) CH_3OH MLs on TiO_2(110), which give the intense experimental peak, at $\varepsilon^{2PP}_{peak} \approx 5.58$ eV relative to the VBM, in the 2PP spectrum[42] shown in Figure 8.

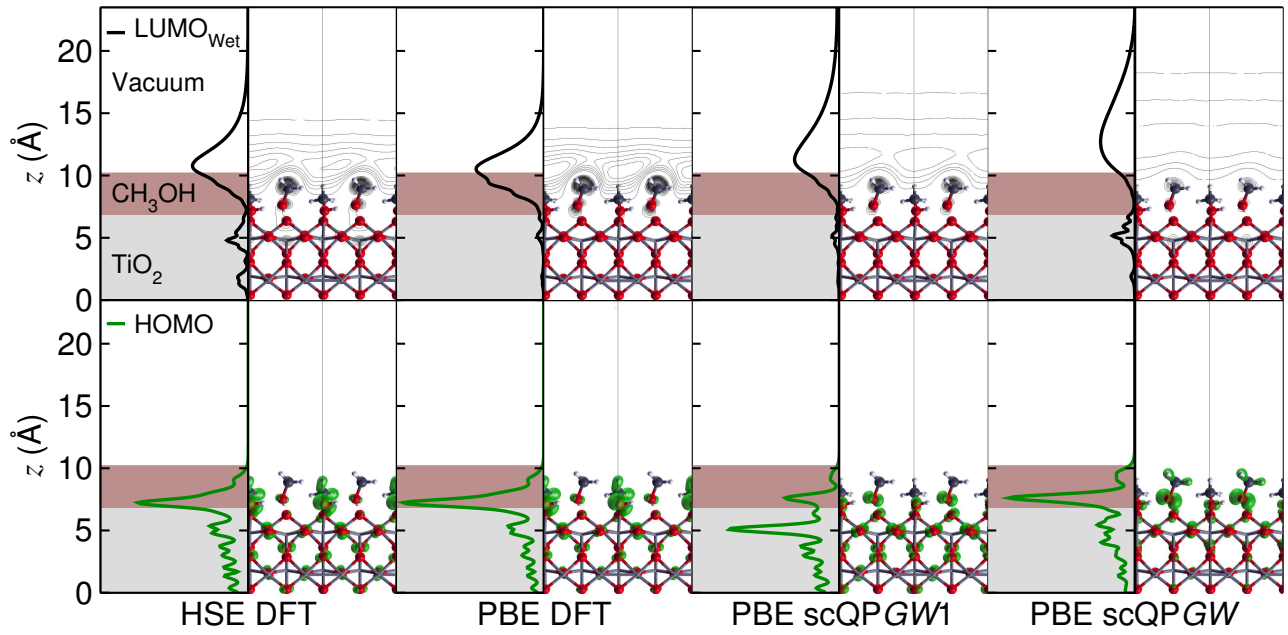

Figure 9. Methanol monolayer on TiO_2(110) HOMO (green isosurfaces) and $LUMO_{Wet}$ (black contour plots) average density in the *xy*-plane,[8] versus distance *z* in Å from the center of the TiO_2 substrate at Γ as obtained from HSE DFT,[64] PBE DFT,[65] PBE scQPGW1,[65] and PBE scQPGW.[64] TiO_2 bulk, CH_3OH molecular layer, and vacuum are depicted by grey, brown, and white regions, respectively. H, C, O, and Ti atoms are represented by white, grey, red, and silver balls, respectively.

As shown in Figure 9, the Wet electron levels are delocalized within the molecular plane with weight inside and above the molecular layer. This means they may be screened based on their density averaged over the *xy*-plane. Specifically, they may be identified as the unoccupied levels with more than half their weight between the bridging O atom of the surface and 5 Å above the top of the molecular layer. It is these levels which are included in the Wet DOS of Figure 8.

On the one hand, DFT underbinds the HOMO levels, which give the highest energy peak in UPS. In particular, we find the PBE HOMO levels are closer to the VBM ($\Delta\varepsilon^{UPS} \approx +0.79$ eV) than those of HSE ($\Delta\varepsilon^{UPS} \approx +0.65$ eV). On the other hand, PBE overbinds the unoccupied Wet levels ($\Delta\varepsilon^{2PP} \approx -0.62$ eV) while HSE underbinds them ($\Delta\varepsilon^{2PP} \approx +0.79$ eV).

Just as PBE underestimates the electronic band gap of the substrate, it also underestimates the CH_3OH HOMO–LUMO energy gap, although to a much smaller extent. HSE provides an excellent description of the electronic properties of the substrate as described in Section 3.2. However, it applies the same screening to all the levels regardless of their nature. More precisely, HSE applies a homogeneous screening, via the macroscopic dielectric constant[3] ($\varepsilon_\infty \sim 4$), throughout the unit cell. This fails to describe the anisotropic screening felt by the molecular levels at the interface. As a result, the unoccupied molecular Wet levels are underbound by HSE. This means HSE is an inappropriate method for molecular/semiconductor interfaces. Instead, QP techniques, where anisotropic screening is calculated directly, should provide a better description of interfacial levels.

The PBE DFT results shown in Figure 8 differ qualitatively from PBE G_0W_0. G_0W_0 shifts the PBE energies of the empty levels up and the occupied molecular levels down, giving near-quantitative agreement with the 2PP and UPS results ($\Delta\varepsilon^{UPS} \approx +0.26$ eV, $\Delta\varepsilon^{2PP} \approx +0.10$ eV). As will be shown in Section 3.4, this improved alignment for the interfacial molecular levels is due to a proper description of the anisotropic screening at the interface.

Although at the G_0W_0 level the vacuum level and wavefunctions are not directly available, the character of the actual and QP wavefunctions is reflected in the experimental spectra and can be inferred from the calculated G_0W_0 PDOS. For example, the HOMO peak in the G_0W_0 PDOS is broadened with respect to the PBE one, in better agreement with experiment (Figure 8). This indicates that the HOMOs of methanol and the O $2p_\pi$ levels[66] of the substrate are more strongly hybridized at the QP level.

The issues with the HSE interfacial level alignment are partially addressed by HSE G_0W_0. G_0W_0 shifts the HSE energies of both the unoccupied and occupied molecular levels down relative to the VBM, giving a better agreement with the 2PP and UPS results ($\Delta\varepsilon^{UPS} \approx +0.05$ eV, $\Delta\varepsilon^{2PP} \approx +0.46$ eV). In fact, G_0W_0 shifts the HSE VBM up in energy, as shown for the bare TiO_2(110) surface in Figures 5 and 6. This is because the QP shifts for bulk, molecular, and vacuum levels are qualitatively different. We will provide a more detailed description in Section 3.4 of the physical origin and nature of the G_0W_0 QP shifts.

To maintain the accurate PBE G_0W_0 description of the spectra while also describing the vacuum level and QP wavefunctions via the self-consistent *GW* procedure, we recently introduced the scQPGW1 approach.[8] The PBE scQPGW1 spectra shown in Figure 8 agree even better than PBE G_0W_0 with the UPS and 2PP measurements ($\Delta\varepsilon^{UPS} \approx -0.15$ eV, $\Delta\varepsilon^{2PP} \approx +0.04$ eV). This suggests that the scQPGW1 QP wavefunction may be more representative of the actual wavefunction.

As shown in Figure 8, scQPGW significantly underbinds the CBM and Wet electron level energies ($\Delta\varepsilon^{2PP} \approx +0.95$ eV), and overbinds the occupied molecular level energies ($\Delta\varepsilon^{UPS} \approx -0.78$ eV). Better agreement is obtained from scQPGW_0, which improves the description of the unoccupied levels ($\Delta\varepsilon^{2PP} \approx +0.33$ eV), but not the occupied molecular levels ($\Delta\varepsilon^{UPS} \approx -0.75$ eV). Although scQPGW_0 reduces the scQPGW band gap by ~ 0.6 eV, the occupied levels have similar energies to scQPGW.

Figure 10 shows the convergence of the CH_3OH PDOS and Wet DOS with respect to the cumulative sum of portions of self energy introduced self-consistently with the QP PBE scQPGW_0 and PBE

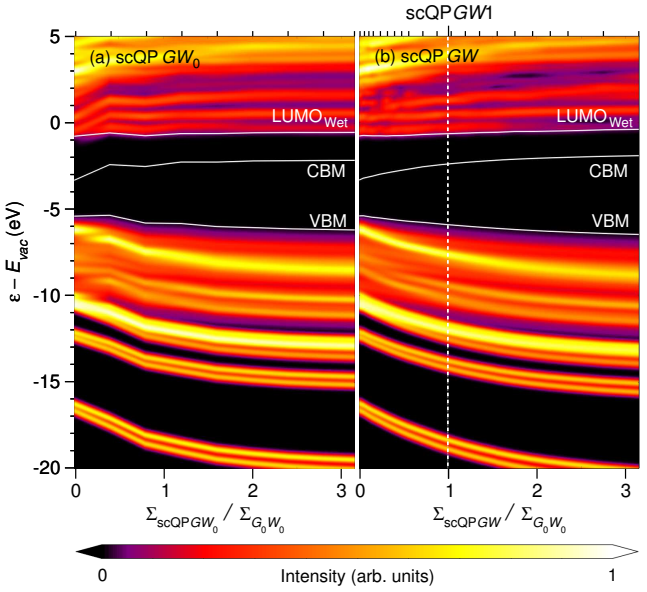

Figure 10. Convergence of the PDOS and Wet DOS for CH_3OH on TiO_2(110) with respect to the cumulative sum of portions of self energy introduced self-consistently, $\Sigma_{scQPGW}/\Sigma_{G_0W_0}$, from (a) PBE scQP$GW_0$ and (b) PBE scQPGW. Energies ε in eV are taken relative to the vacuum level E_{vac}. White solid lines indicate the VBM, CBM, and LUMO$_{Wet}$ positions. White dashed lines indicate the DOS corresponding to scQPGW1 results. Upper ticks indicate the steps of the (a) scQPGW_0 and (b) scQPGW calculations.

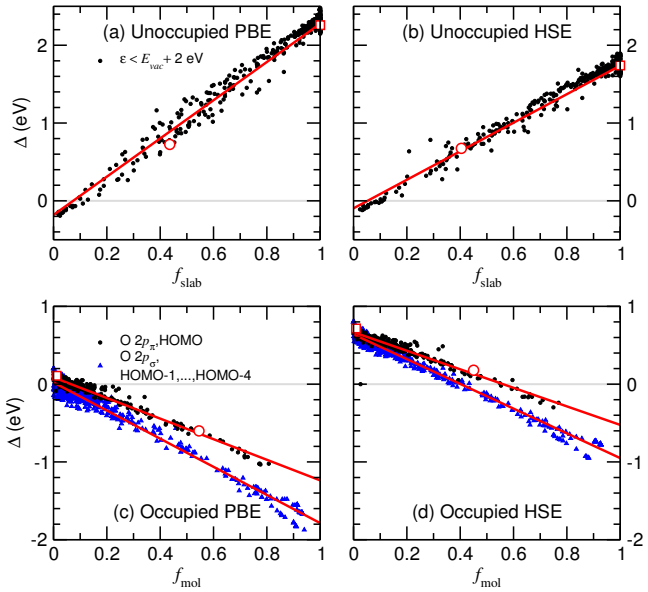

Figure 11. G_0W_0 QP energy correction Δ in eV versus fraction of the wavefunction's density (a,b) in the slab f_{slab} for the unoccupied levels and (c,d) in the molecular layer f_{mol} for the occupied levels from (a,c) PBE[8] and (b,d) HSE for an intact methanol monolayer on TiO_2(110). Open circles denote the (a,b) LUMO$_{Wet}$ and (c,d) HOMO at Γ depicted in Figure 9. Open squares denote the (a,b) CBM and (c,d) VBM levels. Red solid lines are linear fits. (a,c) Adapted with permission from ref. 8. Copyright 2013 American Chemical Society.

scQPGW calculations. As for the bare TiO_2(110) surface, most of the correction to the electronic band gap is already introduced at the scQPGW1 level, i.e. when a total of one full "portion" of self energy has been included within the self-consistent cycles. scQPGW_0 provides a reduced band gap and upshifts the occupied CH_3OH PDOS and downshifts the WET DOS relative to scQPGW. Note that the oscillations observed for scQPGW_0 are related to the use of a larger step size when introducing the portions of self energy.

The QP corrections of the occupied molecular levels follow those of the HOMO levels, with a steeper descent than the VBM. This is qualitatively different from the occupied bulk levels, which follow the VBM. The same behaviour was shown in Figure 6 for the occupied bulk levels of the bare TiO_2(110) surface.

The QP corrections of the Wet electron levels follow the LUMO$_{Wet}$. These corrections are qualitatively different from those of the CBM and have a much "flatter" energy profile. In particular the LUMO$_{Wet}$ energy profile's slope is in between those of the CBM and vacuum levels. These differences in slope are a direct consequence of the anisotropic screening at the interface. In Section 3.4 we will show the G_0W_0 QP corrections are directly correlated with the spacial distribution of the wavefunction.

Overall, we find PBE G_0W_0 and PBE scQPGW1 provide the correct level alignment for methanol on TiO_2(110), while PBE, HSE, HSE G_0W_0, PBE scQPGW, and PBE scQPGW_0 deviate from the UPS or 2PP spectra. At a qualitative level, we find the HOMO energies provide an instructive ordering with decreasing energy of the QP methods: PBE > HSE > PBE G_0W_0 > HSE G_0W_0 > PBE scQPGW1 > PBE scQPGW_0 > PBE scQPGW. The Wet electron energies provide a similar ordering with increasing energy for PBE based QP methods: PBE < PBE G_0W_0 < PBE scQPGW1 < PBE scQPGW_0 < HSE G_0W_0 $\lesssim$ HSE DFT $\lesssim$ PBE scQPGW. As HSE provides the same homogeneous screening to the Wet electron levels and the unoccupied bulk levels, the HSE DFT and HSE G_0W_0 Wet levels are already quite close to the PBE scQPGW results. This reflects both the starting point independence of scQPGW and that HSE provides an electronic structure which is closer to scQPGW than that from PBE.

Next we show how this ordering of the QP techniques is reflected in the spatial distribution of the HOMO wavefunctions shown in Figure 9. The particular HOMO level we consider is the highest energy orbital with $\gtrsim$ 30% of its weight on the atomic orbitals of the molecule. As shown in Figure 9, for HSE and PBE DFT this HOMO level is mostly localized on the methanol molecule closer to the surface, i.e., atop the Ti coordinately unsaturated site (cus).[8] For scQPGW1, the HOMO becomes hybridized with the three-fold coordinated oxygen atoms at the surface and the other methanol molecule. For scQPGW, the weight of the HOMO level is shifted to the other methanol molecule. This reflects both a reordering of the levels, and an increase in hybridization with the bulk levels from the self-consistent QP techniques.

In Figure 9 we also consider how the LUMO$_{Wet}$ wavefunction changes with the level of theory employed. In general, we find the LUMO$_{Wet}$ level becomes increasingly delocalized into the vacuum as one successively moves from PBE to HSE, scQPGW1, and finally scQPGW. By comparing Figures 8 and 9, a correlation is clearly evident between the weight of the LUMO$_{Wet}$ in the vacuum and its energy. Namely, a greater weight of the wavefunction in the vacuum corresponds to a higher peak energy for the Wet DOS. This may be understood as a gradual alignment of the Wet DOS with the vacuum level as the levels become increasingly vacuum like.

At the same time the LUMO$_{Wet}$ wavefunction also becomes increasingly hybridized with the bulk, with HSE being most similar to scQPGW in this respect. Overall, the LUMO$_{Wet}$ levels change from being molecular levels with σ^* character, to increasingly image potential-like vacuum levels at the QP level, as found previously for insulator surfaces.[7]

3.4. Analysis of the QP Corrections for a CH_3OH ML on TiO_2(110). In Section 3.3 we showed that a proper description of

anisotropic screening is necessary to describe level alignment at an interface. Following the analysis of ref. 8, we find the QP G_0W_0 energy corrections may be directly related to the spatial distribution of the wavefunctions.

Figure 11 shows that the QP G_0W_0 energy shifts for (a) PBE and (b) HSE unoccupied levels are proportional to the fraction of the wavefunction within the bulk or molecular layer, i.e., slab, f_{slab}, (gray and brown regions in Figure 9). Similarly, Figure 11 shows that the QP G_0W_0 energy shifts for (c) PBE and (d) HSE occupied levels are proportional to the fraction of the wavefunction within the molecular layer, f_{mol}, (brown region in Figure 9).

For the unoccupied levels, we find for PBE the QP energy shifts are greater for bulk levels than HSE. This is as expected, since a significant portion of the screening is already included within the HSE xc-functional, resulting in a better CBM energy. For vacuum levels there is a small QP shift towards stronger binding with PBE, and essentially no QP shift with HSE. This is because the bare Hartree interaction already describes electron-electron correlation quite well for vacuum levels. Note that the $LUMO_{Wet}$ level (red open circles in Figure 11 (a) and (b)) have nearly equal weights in the slab and vacuum ($f_{slab} \sim 0.4$). This implies the screening felt by these levels is significantly anisotropic. This explains why QP G_0W_0 is needed to properly describe the 2PP spectra.

As shown in Figure 11 (c) and (d), the occupied levels follow two different correlations based on their nature. The TiO_2 O $2p$ level are labelled according to ref. 66. The first correlation includes the weaker bound levels, i.e., the VBM, O $2p_\pi$, and methanol HOMO levels. The second correlation includes more strongly bound levels, i.e., the O $2p_\sigma$, HOMO$-1, \ldots,$ HOMO-4 levels. The correlation is orbital dependent because it is easier to screen σ orbitals, which are located between the atoms, than π orbitals, which are out of plane.[8]

For the occupied bulk levels, we find the QP energy shifts for PBE are almost negligible, while these levels have a significant QP energy shift to weaker binding for HSE. In particular, the HSE VBM is shifted up by about 0.6 eV. This is consistent with what was shown for the bare TiO_2(110) surface in Figure 5. As with the $LUMO_{Wet}$ level, we find the HOMO level (red open circles in Figure 11 (c) and (d)) also have nearly equal weights in the molecular and bulk regions ($f_{mol} \sim 0.5$). This implies the screening felt by these levels is also significantly anisotropic. This explains why QP G_0W_0 is needed to properly describe the UPS spectra. Altogether, these results underline the importance of a proper QP treatment of the anisotropic screening at an interface for the a correct description of interfacial level alignment.

CONCLUSIONS

We have shown that anisotropic screening is an essential component in determining level alignment of photocatalytically active interfacial systems. A proper treatment of the anisotropic screening necessitates the use of QP techniques.

For the CH_3OH ML on TiO_2(110) interface, PBE scQPGW1 is the most accurate technique for reproducing the electronic band gap and the HOMO and $LUMO_{Wet}$ level alignment. In scQPGW1 the xc-potential is entirely replaced by a full portion of self energy during the self-consistent QP procedure. For this reason, the QP energy shifts are quite similar to G_0W_0. Moreover, scQPGW1 gives one access to the QP wavefunctions and vacuum level, which are lacking in G_0W_0. Based on the work of Marques *et al.*, we attribute the excellent performance of PBE G_0W_0 and scQPGW1 to a cancellation of opposite contributions. Specifically, the band gap opening of a fully converged scQPGW calculation is counterbalanced by the band gap reduction due to the lattice polarization contribution to the dielectric function.[3] The latter contribution is especially important for polar materials such as TiO_2.

On the one hand, the HSE G_0W_0 results for the CH_3OH ML on TiO_2(110) interface are closer to the scQPGW than PBE G_0W_0. This means that we do not have this fortuitous error cancellation for the band gap. On the other hand, HSE DFT works well when the screening felt by the wavefunctions is nearly homogeneous. We have shown that this is the case for the VBM and CBM level alignment relative to the vacuum for the bare TiO_2(110). In particular, HSE is able to reproduce the MIES work function.

Finally we have demonstrated that the G_0W_0 QP energy corrections for both PBE and HSE are directly related to the spatial distribution of the wavefunction. Altogether, these calculations provide a new benchmark for the interpretation of MIES, UPS, and 2PP experiments of complex organic molecule–semiconductor interfaces.

AUTHOR INFORMATION

Corresponding Authors

*E-mail: annapaola.migani@cin2.es (A.M.).
*E-mail: duncan.mowbray@gmail.com (D.J.M.).
*E-mail: angel.rubio@ehu.es (A.R.).

Notes

The authors declare no competing financial interest.

ACKNOWLEDGEMENTS

We acknowledge fruitful discussions with Amilcare Iacomino; funding from the European Projects DYNamo (ERC-2010-AdG-267374) and CRONOS (280879-2 CRONOS CP-FP7); Spanish Grants (FIS2012-37549-C05-02, FIS2010-21282-C02-01, PIB2010US-00652, RYC-2011-09582, JAE DOC, JCI-2010-08156); Grupos Consolidados UPV/EHU del Gobierno Vasco (IT-319-07); NSFC (21003113 and 21121003); MOST (2011CB921404); and NSF Grant CHE-1213189; and computational time from i2basque, BSC Red Espanola de Supercomputacion, and EMSL at PNNL by the DOE.

REFERENCES

(1) Henderson, M. A. A surface science perspective on TiO_2 photocatalysis. *Surf. Sci. Rep.* **2011**, *66*, 185–297.
(2) Thompson, T. L.; Yates, J. T. Surface Science Studies of the Photoactivation of TiO_2—New Photochemical Processes. *Chem. Rev.* **2006**, *106*, 4428–4453.
(3) Marques, M. A. L.; Vidal, J.; Oliveira, M. J. T.; Reining, L.; Botti, S. Density-based mixing parameter for hybrid functionals. *Phys. Rev. B* **2011**, *83*, 035119.
(4) Hedin, L. New Method for Calculating the One-Particle Green's Function with Application to the Electron-Gas Problem. *Phys. Rev.* **1965**, *139*, A796–A823.
(5) Onida, G.; Reining, L.; Rubio, A. Electronic excitations: density-functional versus many-body Green's-function approaches. *Rev. Mod. Phys.* **2002**, *74*, 601–659.
(6) Ping, Y.; Rocca, D.; Galli, G. Electronic excitations in light absorbers for photoelectrochemical energy conversion: first principles calculations based on many body perturbation theory. *Chem. Soc. Rev.* **2013**, *42*, 2437–2469.
(7) Rohlfing, M.; Wang, N.-P.; Krüger, P.; Pollmann, J. Image States and Excitons at Insulator Surfaces with Negative Electron Affinity. *Phys. Rev. Lett.* **2003**, *91*, 256802.
(8) Migani, A.; Mowbray, D. J.; Iacomino, A.; Zhao, J.; Petek, H.; Rubio, A. Level Alignment of a Prototypical Photocatalytic System: Methanol on TiO_2(110). *J. Am. Chem. Soc.* **2013**, *135*, 11429–11432.
(9) Migani, A.; Mowbray, D. J. Coverage Dependence of the Level Alignment for Methanol on TiO_2(110). *Comput. Theor. Chem.* **2014**,
(10) Patrick, C. E.; Giustino, F. Quantitative Analysis of Valence Photoemission Spectra and Quasiparticle Excitations at Chromophore-Semiconductor Interfaces. *Phys. Rev. Lett.* **2012**, *109*, 116801.
(11) Freysoldt, C.; Rinke, P.; Scheffler, M. Controlling Polarization at Insulating Surfaces: Quasiparticle Calculations for Molecules Adsorbed on Insulator Films. *Phys. Rev. Lett.* **2009**, *103*, 056803.
(12) Neaton, J. B.; Hybertsen, M. S.; Louie, S. G. Renormalization of Molecular Electronic Levels at Metal-Molecule Interfaces. *Phys. Rev. Lett.* **2006**, *97*, 216405.

(13) Garcia-Lastra, J. M.; Rostgaard, C.; Rubio, A.; Thygesen, K. S. Polarization-induced renormalization of molecular levels at metallic and semiconducting surfaces. *Phys. Rev. B* **2009**, *80*, 245427.
(14) Zhou, C.; Ren, Z.; Tan, S.; Ma, Z.; Mao, X.; Dai, D.; Fan, H.; Yang, X.; LaRue, J.; Cooper, R. *et al.* Site-specific photocatalytic splitting of methanol on TiO_2(110). *Chem. Sci.* **2010**, *1*, 575–580.
(15) Xu, C.; Yang, W.; Ren, Z.; Dai, D.; Guo, Q.; Minton, T. K.; Yang, X. Strong Photon Energy Dependence of the Photocatalytic Dissociation Rate of Methanol on TiO_2(110). *J. Am. Chem. Soc.* **2013**, *135*, 19039–19045.
(16) Xu, C.; Yang, W.; Guo, Q.; Dai, D.; Chen, M.; Yang, X. Molecular Hydrogen Formation from Photocatalysis of Methanol on TiO_2(110). *J. Am. Chem. Soc.* **2013**, *135*, 10206–10209.
(17) Guo, Q.; Xu, C.; Ren, Z.; Yang, W.; Ma, Z.; Dai, D.; Fan, H.; Minton, T. K.; Yang, X. Stepwise Photocatalytic Dissociation of Methanol and Water on TiO_2(110). *J. Am. Chem. Soc.* **2012**, *134*, 13366–13373.
(18) Phillips, K. R.; Jensen, S. C.; Baron, M.; Li, S.-C.; Friend, C. M. Sequential Photo-oxidation of Methanol to Methyl Formate on TiO_2(110). *J. Am. Chem. Soc.* **2013**, *135*, 574–577.
(19) Yuan, Q.; Wu, Z.; Jin, Y.; Xu, L.; Xiong, F.; Ma, Y.; Huang, W. Photocatalytic Cross-Coupling of Methanol and Formaldehyde on a Rutile TiO_2(110) Surface. *J. Am. Chem. Soc.* **2013**, *135*, 5212–5219.
(20) Kawai, T.; Sakata, T. Photocatalytic hydrogen production from liquid methanol and water. *J. Chem. Soc., Chem. Commun.* **1980**, 694–695.
(21) Fujishima, A.; Honda, K. Electrochemical Photolysis of Water at a Semiconductor Electrode. *Nature* **1972**, *238*, 37–38.
(22) Fujishima, A.; Zhang, X.; Tryk, D. A. TiO_2 photocatalysis and related surface phenomena. *Surf. Sci. Rep.* **2008**, *63*, 515–582.
(23) Onishi, H.; Aruga, T.; Egawa, C.; Iwasawa, Y. Adsorption of CH_3OH, HCOOH and SO_2 on TiO_2(110) and stepped TiO_2(441) surfaces. *Surf. Sci.* **1988**, *193*, 33–46.
(24) Li, B.; Zhao, J.; Onda, K.; Jordan, K. D.; Yang, J.; Petek, H. Ultrafast Interfacial Proton-Coupled Electron Transfer. *Science* **2006**, *311*, 1436–1440.
(25) Onda, K.; Li, B.; Zhao, J.; Jordan, K. D.; Yang, J.; Petek, H. Wet Electrons at the H_2O/TiO_2(110) Surface. *Science* **2005**, *308*, 1154–1158.
(26) Henderson, M. A.; Lyubinetsky, I. Molecular-Level Insights into Photocatalysis from Scanning Probe Microscopy Studies on TiO_2(110). *Chem. Rev.* **2013**, *113*, 4428–4455.
(27) Shen, M.; Acharya, D. P.; Dohnálek, Z.; Henderson, M. A. Importance of Diffusion in Methanol Photochemistry on TiO_2(110). *J. Phys. Chem. C* **2012**, *116*, 25465–25469.
(28) Shen, M.; Henderson, M. A. Identification of the Active Species in Photochemical Hole Scavenging Reactions of Methanol on TiO_2. *J. Phys. Chem. Lett.* **2011**, *2*, 2707–2710.
(29) Zhao, J.; Yang, J.; Petek, H. Theoretical study of the molecular and electronic structure of methanol on a TiO_2(110) surface. *Phys. Rev. B* **2009**, *80*, 235416.
(30) Shishkin, M.; Kresse, G. Implementation and performance of the frequency-dependent *GW* method within the PAW framework. *Phys. Rev. B* **2006**, *74*, 035101.
(31) van Schilfgaarde, M.; Kotani, T.; Faleev, S. Quasiparticle Self-Consistent *GW* Theory. *Phys. Rev. Lett.* **2006**, *96*, 226402.
(32) Kotani, T.; van Schilfgaarde, M.; Faleev, S. V.; Chantis, A. Quasiparticle self-consistent GW method: a short summary. *J. Phys. Condens. Mat.* **2007**, *19*, 365236.
(33) Shishkin, M.; Marsman, M.; Kresse, G. Accurate Quasiparticle Spectra from Self-Consistent *GW* Calculations with Vertex Corrections. *Phys. Rev. Lett.* **2007**, *99*, 246403.
(34) Shishkin, M.; Kresse, G. Self-consistent *GW* calculations for semiconductors and insulators. *Phys. Rev. B* **2007**, *75*, 235102.
(35) Perdew, J. P.; Zunger, A. Self-interaction correction to density-functional approximations for many-electron systems. *Phys. Rev. B* **1981**, *23*, 5048–5079.
(36) Perdew, J. P.; Burke, K.; Ernzerhof, M. Generalized Gradient Approximation Made Simple. *Phys. Rev. Lett.* **1996**, *77*, 3865.
(37) Heyd, J.; Scuseria, G. E.; Ernzerhof, M. Hybrid functionals based on a screened Coulomb potential. *J. Chem. Phys.* **2003**, *118*, 8207.
(38) Data taken from the supporting information of ref. 8.
(39) Cardona, M.; Harbeke, G. Optical Properties and Band Structure of Wurtzite-Type Crystals and Rutile. *Phys. Rev.* **1965**, *137*, A1467–A1476.
(40) Tiwald, T. E.; Schubert, M. Measurement of rutile TiO_2 dielectric tensor from 0.148 to 33 μm using generalized ellipsometry. *Proc. SPIE* **2000**, *4103*, 19–29.
(41) Borodin, A.; Reichling, M. Characterizing TiO_2(110) surface states by their work function. *Phys. Chem. Chem. Phys.* **2011**, *13*, 15442–15447.
(42) Onda, K.; Li, B.; Zhao, J.; Petek, H. The electronic structure of methanol covered TiO_2(110) surfaces. *Surf. Sci.* **2005**, *593*, 32–37.
(43) Zhou, C.; Ma, Z.; Ren, Z.; Wodtke, A. M.; Yang, X. Surface photochemistry probed by two-photon photoemission spectroscopy. *Energy Environ. Sci.* **2012**, *5*, 6833–6844.
(44) Caruso, F.; Rinke, P.; Ren, X.; Scheffler, M.; Rubio, A. Unified description of ground and excited states of finite systems: The self-consistent *GW* approach. *Phys. Rev. B* **2012**, *86*, 081102.
(45) Botti, S.; Marques, M. A. L. Strong Renormalization of the Electronic Band Gap due to Lattice Polarization in the *GW* Formalism. *Phys. Rev. Lett.* **2013**, *110*, 226404.
(46) Chiodo, L.; García-Lastra, J. M.; Iacomino, A.; Ossicini, S.; Zhao, J.; Petek, H.; Rubio, A. Self-energy and excitonic effects in the electronic and optical properties of TiO_2 crystalline phases. *Phys. Rev. B* **2010**, *82*, 045207.
(47) Kang, W.; Hybertsen, M. S. Quasiparticle and optical properties of rutile and anatase TiO_2. *Phys. Rev. B* **2010**, *82*, 085203.
(48) Landmann, M.; Rauls, E.; Schmidt, W. G. The electronic structure and optical response of rutile, anatase and brookite TiO_2. *J. Phys.: Condens. Matter* **2012**, *24*, 195503.
(49) van Setten, M. J.; Gremaud, R.; Brocks, G.; Dam, B.; Kresse, G.; de Wijs, G. A. Optical response of the sodium alanate system: GW_0-BSE calculations and thin film measurements. *Phys. Rev. B* **2011**, *83*, 035422.
(50) Reining, L.; Olevano, V.; Rubio, A.; Onida, G. Excitonic Effects in Solids Described by Time-Dependent Density-Functional Theory. *Phys. Rev. Lett.* **2002**, *88*, 066404.
(51) Kresse, G.; Joubert, D. From ultrasoft pseudopotentials to the projector augmented-wave method. *Phys. Rev. B* **1999**, *59*, 1758.
(52) Kresse, G.; Furthmüller, J. Efficient iterative schemes for ab initio total-energy calculations using a plane-wave basis set. *Phys. Rev. B* **1996**, *54*, 11169.
(53) Mortensen, J. J.; Hansen, L. B.; Jacobsen, K. W. Real-space grid implementation of the projector augmented wave method. *Phys. Rev. B* **2005**, *71*, 035109.
(54) Enkovaara, J.; Rostgaard, C.; Mortensen, J. J.; Chen, J.; Dulak, M.; Ferrighi, L.; Gavnholt, J.; Glinsvad, C.; Haikola, V.; Hansen, H. A. *et al.* Electronic structure calculations with GPAW: a real-space implementation of the projector augmented-wave method. *J. Phys. Condens. Mat.* **2010**, *22*, 253202.
(55) Burdett, J. K.; Hughbanks, T.; Miller, G. J.; Richardson, J. W.; Smith, J. V. Structural-electronic relationships in inorganic solids: powder neutron diffraction studies of the rutile and anatase polymorphs of titanium dioxide at 15 and 295 K. *J. Am. Chem. Soc.* **1987**, *109*, 3639–3646.
(56) Sato, N. *Electrochemistry at Metal and Semiconductor Electrodes*; Elsivier Science & Technology: Oxford, 1998.
(57) Aono, M.; Hasiguti, R. R. Interaction and ordering of lattice defects in oxygen-deficient rutile TiO_{2-x}. *Phys. Rev. B* **1993**, *48*, 12406–12414.
(58) Yamakata, A.; Ishibashi, T.; Onishi, H. Kinetics of the photocatalytic water-splitting reaction on TiO_2 and Pt/TiO_2 studied by time-resolved infrared absorption spectroscopy. *J. Mol. Catal. A: Chem.* **2003**, *199*, 85–94.
(59) Chung, Y. W.; Lo, W. J.; Somorjai, G. A. Low energy electron diffraction and electron spectroscopy studies of the clean (110) and (100) titanium dioxide (rutile) crystal surfaces. *Surf. Sci.* **1977**, *64*, 588.
(60) Onda, K.; Li, B.; Petek, H. Two-photon photoemission spectroscopy of TiO_2(110) surfaces modified by defects and O_2 or H_2O adsorbates. *Phys. Rev. B* **2004**, *70*, 045415.
(61) Tezuka, Y.; Shin, S.; Ishii, T.; Ejima, T.; Suzuki, S.; Sato, S. Photoemission and Bremsstrahlung Isochromat Spectroscopy Studies of TiO_2 (Rutile) and $SrTiO_3$. *J. Phys. Soc. Jpn.* **1994**, *63*, 347–357.
(62) Traylor, J. G.; Smith, H. G.; Nicklow, R. M.; Wilkinson, M. K. Lattice Dynamics of Rutile. *Phys. Rev. B* **1971**, *3*, 3457–3472.
(63) Lee, B.; ki Lee, C.; Hwang, C. S.; Han, S. Influence of exchange-correlation functionals on dielectric properties of rutile TiO_2. *Curr. Appl. Phys.* **2011**, *11*, S293–S296.
(64) $LUMO_{Wet}$ average density in the *xy*-plane from supporting information of ref. 8.
(65) HOMO and $LUMO_{Wet}$ average densities in the *xy*-plane from ref. 8.
(66) Mowbray, D. J.; Martínez, J. I.; Calle-Vallejo, F.; Rossmeisl, J.; Thygesen, K. S.; Jacobsen, K. W.; Nørskov, J. K. Trends in Metal Oxide Stability for Nanorods, Nanotubes, and Surfaces. *J. Phys. Chem. C* **2011**, *115*, 2244–2252.